Springer

Journal of Mechanical Science and Technology 22 (2008) 1612~1619

Journal of Mechanical Science and Technology

www.springerlink.com/content/1738-494x
DOI 10.1007/s12206-008-0504-8

Spectral element modeling and analysis of the blood flow through a human blood vessel

Usik Lee*, Bosung Seo and Injoon Jang
Department of Mechanical Engineering, Inha University 253 Yonghyun-Dong, Nam-Gu, Inchon 402-751, South Korea

(Manuscript Received March 6, 2007; Revised January 14, 2008; Accepted May 9, 2008)

Abstract

As the blood flow characteristics are closely related to various cardiovascular diseases, it is very important to predict them accurate enough in an efficient way. Thus, this paper proposes a one-dimensional spectral element model for human blood vessels with varying cross-sections. The spectral element model is formulated by using the variational approach of finite element formulation. The wave solutions analytically solved in the frequency-domain to satisfy governing equations are used to determine the frequency-dependent interpolation functions. The spectral finite element model is then applied to an example blood vessel to investigate the blood flow rate and blood pressure through the blood vessel.

Keywords: Blood vessel; Spectral element method; Spectral element model; Blood pressure; Blood flow rate

1. Introduction

The blood flow characteristics determine the wall shear stress and wall tension. As the wall shear stress and wall tension are closely related to the cardiovascular diseases such as stenosis and aneurysm, it is very important to predict the blood flow characteristics accurately in an efficient way for the cardiovascular disease research, medical devise design and surgical planning. To this end, computational methods have merged as the powerful tools for the modeling and analysis of the blood flow and pressure in arteries.

Modeling of blood flow and pressure has been studied intensively over the years, and various computational models have been reported [1-8]. The one-dimensional (1D) models have been widely used because they can provide clinically relevant information on local mean blood flow and pressure waves through arterial systems very efficiently as well as the boundary conditions suitable for three-dimensional (3D) models [4, 5]. For solving 1D models of blood flow, the two-step Lax-Wendroff method [3] and finite element method (FEM) [6-8] have been applied. The 1D modeling of a vascular network in space-time variables was also considered by Sherwin et al. [9]. However, to the authors' best knowledge, the spectral element method (SEM) has never been applied to the modeling and analysis of the blood flows through human blood vessels.

The FEM is certainly a very powerful tool for solving diverse complex engineering problems. However, as the simple polynomials which are not related to the frequency of vibration are used as the interpolation functions to formulate the conventional finite element models, it is often inevitable to use very fine meshes to improve the FEM solutions, especially at high frequency. This may increase the computation cost significantly. In contrast to FEM, the spectral element method (SEM) is known as an exact element method because the exact wave solutions satisfying governing equations of motion in the frequency-domain are used as the frequency-dependent interpolation functions to formulate spectral finite element models [10, 11]. Thus, SEM may allow us to get very accurate dynamic response for a 1D structure by modeling the

*Corresponding author. Tel.: +82 32 860 7318, Fax.: +82 32 866 1434
E-mail address: ulee@inha.ac.kr

whole structure of any length as a single element in the absence of any discontinuity or irregularity in geometrical and material properties, which may benefit us to drastically reduce the computation cost.

As the SEM has never been applied to the modeling and analysis of the blood flows, the purposes of this paper are: (1) to develop a spectral element model for the blood flows through human blood vessels by improving the previous study [12], and (2) to apply the spectral element model to investigate the blood flow characteristics for various velocity profiles of blood flow.

2. Governing equations

The 1D theory of arterial flow consists of a continuity equation, an axial momentum balance equation, and a constitutive equation for the flow in an impermeable, deforming, elastic domain as [2, 3]:

$$\dot{S} + Q' = 0 \tag{1}$$

$$\dot{Q} + (1+\Delta)(Q^2/S) + (S/\rho)P' = \nu H(Q/S) + \nu Q'' \tag{2}$$

$$P\left(S(x,t),x,t\right) = P_d + (4/3)\left(Eh/r_d\right)\left(1 - \sqrt{S_d/S(x,t)}\right) \tag{3}$$

where S is the cross-sectional area, Q is the volumetric flow rate, P is the pressure, ρ is the mass density of blood, ν is the kinematic viscosity of blood, E is the Young's modulus of blood vessel, and h is the wall thickness of blood vessel. S_d and r_d are the uniform cross-sectional area and radius at diastole pressure P_d = 80 mmHg. The parameters Δ and H are determined by the blood flow velocity profile over the cross-section of a blood vessel [2, 3]: $\Delta = 0$ and $H = 0$ for the uniform flow (Fig. 1a); $\Delta = 1/3$ and $H = 8\pi$ for the parabolic flow (Fig. 1b); $\Delta = (2/3)\delta/r_d = 0.0667$ and $H = 2\pi r_d/\delta = 20\pi$ for the boundary layer flow, where δ denotes the boundary layer thickness (Fig. 1c). Note that the dot and the prime represent the derivative with respect to time t and coordinate x, respectively. Olufsen [3] derived the empirical expression for Eh/r_d in the constitutive equation as follows:

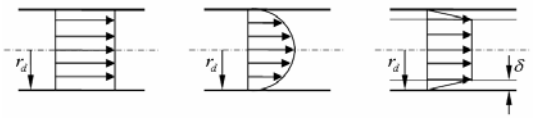

(a) (b) (c)

Fig. 1. Types of blood flow velocity profiles over the cross-section of a blood vessel: (a) uniform flow, (b) parabolic flow, and (c) boundary layer (BL) flow.

$$Eh/r_d = k_1 exp(k_2 r_d) + k_3 \tag{4}$$

where $k_1 = 2\times10^7$ g·s^{-2}·cm^{-1}, k_2 = - 22.53 cm^{-1}, and $k_3 = 8.65\times10^5$ g·s^{-2}·cm^{-1} [3, 7].

Assume that the blood pressure and cross-sectional area can be written as

$$S(x,t) = S_d(x) + s(x,t), \quad P(x,t) = P_d + p(x,t) \tag{5}$$

where $s(x, t)$ and $p(x, t)$ are the small perturbations with respect to the values at diastole phase. The cross-sectional area at the diastole phase is assumed to vary as

$$S_d(x) = S_0(1-\theta x) \quad (\theta x < 1) \tag{6}$$

where S_0 is the cross-sectional area at the inlet of an blood vessel and θ is the parameter which represents the taper of the blood vessel.

Substitute Eq. (5) into Eq. (3) and then apply Eqs. (4) and (6) to get

$$p(x,t) \cong \left(2Eh/3r_d\right)\left(s/S_d\right) \cong \alpha\left(s/S_0\right) \tag{7}$$

Where

$$\alpha = 2Eh/3r_d = (2/3)[k_1 \exp(k_2 r_d) + k_3] \tag{8}$$

Substituting Eq. (5) into Eqs. (1) and (2), we get approximated expressions as

$$\dot{s} + Q' \cong 0 \tag{9}$$

$$\dot{Q} + (1+\Delta)\left[\left(Q^2/S_d\right)\left(1 - s/S_d\right)\right] + \left[\left(S_d + s\right)/\rho\right]p' \cong \nu H\left(Q/S_d\right)\left(1 - s/S_d\right) + \nu Q'' \tag{10}$$

Applying Eq. (7) into Eqs. (9) and (10) to replace $s(x, t)$ with $p(x, t)$ and then using the assumptions $S_d > s(x, t)$ and $\theta x < 1$, we can get simplified continuity and momentum equations as

$$a_0\dot{p} + a_1 Q' = 0 \tag{11}$$

$$a_0 p' + \dot{Q} + a_2 Q - a_3 Q'' = f(x,t) \tag{12}$$

where

$$f(x,t) = -a_4 QQ' + a_5 pQ - a_6 p'p + a_7 pQQ' + a_8 p'Q^2 - a_9 Q^2 + a_{10} pQ^2 \tag{13}$$

And

$$\begin{aligned} &a_0 = S_0/\rho, \quad a_1 = \alpha/\rho, \quad a_2 = \nu H/S_0 \\ &a_3 = \nu, \qquad\qquad a_4 = 2(1+\Delta)/S_0 \\ &a_5 = \nu H/(\alpha S_0), \qquad a_6 = S_0/(\alpha\rho) \\ &a_7 = 2(1+\Delta)/(\alpha S_0), \quad a_8 = (1+\Delta)/(\alpha S_0) \\ &a_9 = (1+\Delta)\theta/S_0, \qquad a_{10} = (1+\Delta)\theta/\alpha S_0 \end{aligned} \tag{14}$$

Note that all nonlinear terms are collected in the right-hand side of Eq. (12) and denoted by the function $f(x, t)$. When compared with the previous study [12], one may find that the last two terms of Eq. (13) are newly added. The function $f(x, t)$ will be considered as the pseudo-force for the application of an iterative method for nonlinear problems.

3. Spectral Element Model

3.1 Weak forms in the frequency domain

We basically follow the same procedure of spectral element formulation as used in the previous study [12]. Based on the discrete Fourier transform (DFT) theory [13], we first assume the time histories of $p(x, t)$, $Q(x, t)$, and $f(x, t)$ in the spectral forms as

$$p(x,t) = \frac{1}{N}\sum_{n=0}^{N-1} \bar{p}_n(x) e^{i\omega_n t} \tag{15}$$

$$Q(x,t) = \frac{1}{N}\sum_{n=0}^{N-1} \bar{Q}_n(x) e^{i\omega_n t} \tag{16}$$

$$f(x,t) = \frac{1}{N}\sum_{n=0}^{N-1} \bar{f}_n(x) e^{i\omega_n t} \tag{17}$$

where $\bar{p}_n(x)$, $\bar{Q}_n(x)$, and $\bar{f}_n(x)$ are the Fourier components of $p(x,t)$, $Q(x,t)$, and $f(x,t)$, respectively; $\omega_n = 2\pi n/T$ (n = 0,1,2,…, N) where T is the period and N is the number of samples defined in the DFT theory [13].

Substitution of Eqs. (15-17) into Eqs. (11) and (12) yields the governing equations for $\bar{Q}_n(x)$ and $\bar{p}_n(x)$ as

$$c_n^2 \bar{Q}_n'' + \omega_n^2 (1 - i\eta_n)\bar{Q}_n + \sigma_{1n}\bar{f}_n = 0 \tag{18}$$

$$c_n^2 \bar{p}_n'' + \omega_n^2 (1 - i\eta_n)\bar{p}_n + \sigma_{2n}\bar{g}_n = 0 \tag{19}$$

where $\bar{g}_n(x)$ are the Fourier components of $g(x, t) = f'(x, t)$ and the following definitions are used.

$$\begin{aligned} &c_n = \sqrt{\frac{a_1^2 + \omega_n^2 a_3^2}{a_1 - a_2 a_3}}, \quad \eta_n = \frac{\omega_n^2 a_3 + a_1 a_2}{\omega_n (a_1 - a_2 a_3)} \\ &\sigma_{1n} = \frac{\omega_n^2 a_3}{a_1 - a_2 a_3}\left\{1 + i\left(\frac{a_1}{\omega_n a_3}\right)\right\}, \quad \sigma_{2n} = -\frac{a_1(a_1 - i\omega_n a_3)}{a_0(a_1 - a_2 a_3)} \end{aligned} \tag{20}$$

Multiplying Eq. (18) by $\delta\bar{Q}_n(x)$, and Eq. (19) by $\delta\bar{p}_n(x)$, and then integrating by parts, and finally using the relation $i\omega_n a_0 \bar{p}_n + \bar{Q}_n' = 0$ derived from Eq. (11), we obtain the weak forms as follows:

$$\begin{aligned} &\int_0^l c_n^2 \bar{Q}_n' \delta\bar{Q}_n' dx - \int_0^l \omega_n^2 (1 - i\eta_n)\bar{Q}_n \delta\bar{Q}_n dx \\ &+ \int_0^l \sigma_{1n}\bar{f}_n \delta\bar{Q}_n dx + i\omega_n c_n^2 a_0 \bar{p}_n \delta\bar{Q}_n\Big|_0^l = 0 \end{aligned} \tag{21}$$

$$\begin{aligned} &\int_0^l c_n^2 \bar{p}_n' \delta\bar{p}_n' dx - \int_0^l \omega_n^2 (1 - i\eta_n)\bar{p}_n \delta\bar{p}_n dx \\ &- \int_0^l \sigma_{2n}\bar{g}_n \delta\bar{p}_n dx - c_n^2 \bar{p}_n' \delta\bar{p}_n\Big|_0^l = 0 \end{aligned} \tag{22}$$

Consider a function $z_3(x, t)$ defined by the multiplication of two functions $z_1(x, t)$ and $z_2(x, t)$ as

$$z_3(x,t) = z_1(x,t) z_2(x,t) \tag{23}$$

Define $\bar{Z}_n^1(x)$, $\bar{Z}_n^2(x)$ and $\bar{Z}_n^3(x)$ as the Fourier components of $z_1(x,t)$, $z_2(x,t)$ and $z_3(x,t)$, respectively. Then, by applying the DFT theory to Eq. (23), one can obtain the relation as

$$\bar{Z}_n^3(x) = \frac{1}{N}\left(\sum_{j=0}^{n} \bar{Z}_j^1(x)\bar{Z}_{n-j}^2(x) + \sum_{j=n+1}^{N-1} \bar{Z}_j^1(x)\bar{Z}_{N+n-j}^2(x)\right) \tag{24}$$

The Fourier components $\bar{f}_n(x)$ of the pseudo-force $f(x, t)$, which is the nonlinear function of $p(x, t)$ and $Q(x, t)$, can be expressed in terms of $\bar{p}_n(x)$ and $\bar{Q}_n(x)$ by repeatedly applying the formula, Eq. (24), to each nonlinear term in $f(x,t)$.

3.2 Spectral element formulation

To formulate the spectral element, we consider the linear homogeneous governing equations reduced from Eqs. (18) and (19) as

$$c_n^2 \bar{Q}_n'' + \omega_n^2 (1 - i\eta_n) \bar{Q}_n = 0 \tag{25}$$

$$c_n^2 \bar{p}_n'' + \omega_n^2 (1 - i\eta_n) \bar{p}_n = 0 \tag{26}$$

with the relevant boundary conditions

$$\bar{Q}_n(0) = \bar{Q}_{n1}, \ \bar{Q}_n(l) = \bar{Q}_{n2}, \ \bar{p}_n(0) = \bar{p}_{n1}, \ \bar{p}_n(l) = \bar{p}_{n2} \tag{27}$$

The solutions of Eqs. (25) and (26) can be obtained in terms of the dynamic shape function matrix $\boldsymbol{N}(x, \omega_n)$ and the nodal degrees of freedom (DOFs) $\bar{\boldsymbol{Q}}_n = \{\bar{Q}_{n1} \ \ \bar{Q}_{n2}\}^{\mathrm{T}}$ and $\bar{\boldsymbol{p}}_n = \{\bar{p}_{n1} \ \ \bar{p}_{n2}\}^{\mathrm{T}}$ as

$$\begin{aligned} \bar{Q}_n(x) &= \left[\mathbf{N}(x, \omega_n)\right]\left\{\bar{\boldsymbol{Q}}_n\right\} \\ \bar{p}_n(x) &= \left[\mathbf{N}(x, \omega_n)\right]\left\{\bar{\boldsymbol{p}}_n\right\} \end{aligned} \tag{28}$$

where

$$\begin{aligned} &[\boldsymbol{N}(x, \omega_n)] = [\csc(k_n l)\sin(k_n l - k_n x) \ \ \csc(k_n l)\sin(k_n x)] \\ &k_n = (\omega_n / c_n)\sqrt{1 - i\eta_n} \end{aligned} \tag{29}$$

Substitution of Eq. (28) into Eqs. (21) and (22) gives

$$\left[\boldsymbol{S}(\omega_n)\right]\left\{\bar{\boldsymbol{Q}}_n\right\} = \left\{\bar{\boldsymbol{f}}_{1n}\right\} + \left\{\bar{\boldsymbol{F}}_{1n}\right\} \tag{30}$$

and

$$\left[\boldsymbol{S}(\omega_n)\right]\left\{\bar{\boldsymbol{p}}_n\right\} = \left\{\bar{\boldsymbol{f}}_{2n}\right\} + \left\{\bar{\boldsymbol{F}}_{2n}\right\} \tag{31}$$

where

$$\begin{aligned} &\left[\boldsymbol{S}(\omega_n)\right] = c_n^2 \int_0^l \left[\boldsymbol{N}'\right]^{\boldsymbol{T}} \left[\boldsymbol{N}'\right] dx - \omega_n^2 (1 - i\eta_n) \int_0^l \left[\boldsymbol{N}\right]^{\boldsymbol{T}} \left[\boldsymbol{N}\right] dx \\ &\left\{\bar{\boldsymbol{f}}_{1n}(Q, p)\right\} \cong \sigma_{1n} \bar{f}_n(x_c) \int_0^l \left[\boldsymbol{N}\right]^{\boldsymbol{T}} dx \\ &\left\{\bar{\boldsymbol{F}}_{1n}\right\} = i\omega_n c_n^2 a_0 \left\{\bar{\boldsymbol{p}}_n\right\} \\ &\left\{\bar{\boldsymbol{f}}_{2n}(Q, p)\right\} \cong \sigma_{2n} \bar{g}_n(x_c) \int_0^l \left[\boldsymbol{N}\right]^{\boldsymbol{T}} dx \\ &\left\{\bar{\boldsymbol{F}}_{2n}\right\} = i\omega_n c_n^2 a_0^{-1} \left\{\bar{\boldsymbol{Q}}_n\right\} \end{aligned} \tag{32}$$

The matrix $[\boldsymbol{S}(\omega_n)]$ is the spectral element matrix which is frequency dependent. The spectral element equations, Eq. (30) and Eq. (31), can be combined and assembled in the exactly same way as used in the conventional FEM, followed by the application of relevant boundary conditions [10, 11].

The terms in the right-hand sides of Eqs. (30) and (31) contain unknown Fourier spectra $\bar{\boldsymbol{p}}_n$ and $\bar{\boldsymbol{Q}}_n$. Thus, we need to solve Eqs. (30) and (31) for $\bar{\boldsymbol{p}}_n$ and $\bar{\boldsymbol{Q}}_n$ by using an iterative method. Once $\bar{\boldsymbol{p}}_n$ and $\bar{\boldsymbol{Q}}_n$ are computed, we compute the Fourier spectra $\bar{p}_n(x)$ and $\bar{Q}_n(x)$ at an arbitrary location x from Eq. (28). Finally, we compute the time histories of $p(x, t)$ and $Q(x, t)$ from Eq. (15) and Eq. (16), respectively, based on the DFT theory. In SEM, the computation of time histories is efficiently conducted by using the inverse fast Fourier transform (FFT) algorithm [10, 11].

4. Numerical results and discussion

The spectral element model developed in this paper is applied to a blood vessel of length L as shown in Fig. 2, where r_0 = 1.25 cm. The blood properties are given by ρ = 1.055 g/cm^3 and ν = 0.046 cm^2/s. The blood flow rate and pressure are computed by assuming that the pulsatile blood flow rate at the inlet (i.e., x = 0 cm) is given by Fig. 3 and the perturbed blood pressure at the inlet is zero, i.e., $p(x, t)$ = 0 mmHg or $P(0, t)$ = 80 mmHg. Fig. 1 shows the blood flow velocity profiles over the cross-section of the blood vessel, which are considered for numerical computations in this study: uniform flow, parabolic flow and boundary layer (BL) flow (uniform flow in the core region and linear velocity profile in the boundary layer). The numerical results obtained by using the present spectral element model are displayed in Fig. 4 through Fig. 9. To compute the time histories of blood flow rate and pressure, N = 2^{13} (the number of samples) is used for the FFT and inverse FTT applications.

Fig. 4 shows the blood flow rate and the perturbed blood pressure at the distance of 3.5 cm from the inlet of blood vessel (i.e., x = 3.5 cm) when the uniform flow profile is used. Because the blood flow rate specified at the inlet of blood vessel is pulsatile, the

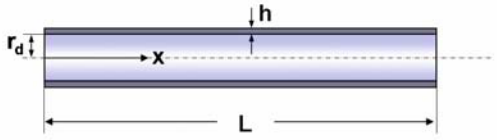

Fig. 2. The geometry of a blood vessel.

blood flow rate and the (perturbed) blood pressure predicted at x = 3.5 cm are also pulsatile. The predicted perturbed blood pressure has a value between 0 mmHg and 40 mmHg: this means that the blood pressure of a healthy person is between 80 mmHg and 120 mmHg.

First, to evaluate the high accuracy of the present spectral element model, the blood flow rates and blood pressures computed by using the present SEM

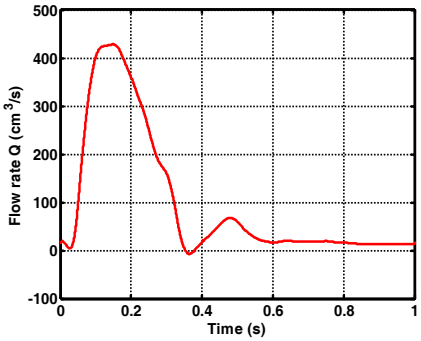

Fig. 3. The blood flow rate at the inlet of an example blood vessel considered for numerical computation.

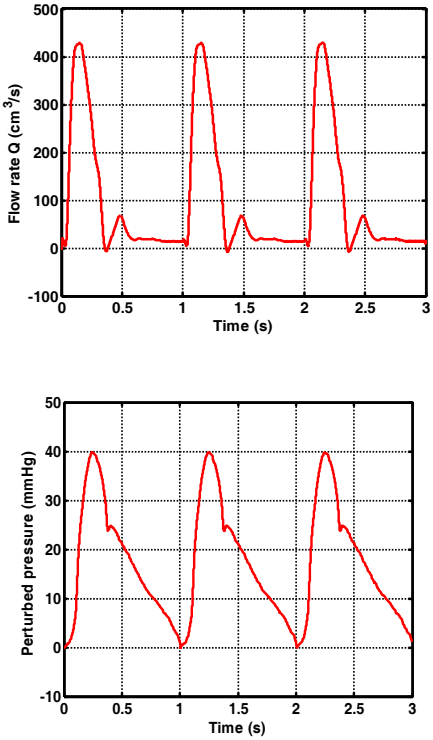

Fig. 4. The blood flow rate and perturbed blood pressure at x = 3.5 cm for the uniform flow.

are compared with those computed by using the FEM model formulated in this study. The FEM model is given in Appendix A. To get the FEM results shown in Fig. 5, the Runge-Kutta algorithm of MATLAB is used with a time-step size of 0.01 seconds, which is chosen to provide sufficiently converged reliable solutions. As shown in Fig. 5, only two finite elements are used for the SEM, while the number of finite elements is increased for the conventional FEM to get improved results. As the extremely high accuracy of SEM has been already proved in many related articles, Fig. 5 certainly shows that FEM results converge to SEM results as the number of finite elements used in the conventional FEM is increased. Based on the proof of the high accuracy of the present spectral element model, spectral element analyses are conducted to investigate the blood flow through the example blood vessel, and their results are displayed in Fig. 6 through Fig. 8 for the case of uniform flow.

Fig. 6 shows the effects of the taper of the varying cross-section of blood vessel on the blood pressure. A blood vessel with narrowing cross-section has lower blood pressure than one with uniform cross-section. This is true because the flow velocity must increase to make an input quantity of blood flow through the narrow cross-section, which may in turn decrease the pressure by Bernoulli's principle.

Fig. 7 compares the perturbed blood pressures at three different locations: x = 0 cm, 3.5 cm, and 7 cm. It is obvious from Fig. 7 that the blood pressure at farther distance is delayed due to the distance between chosen locations. We can also observe from

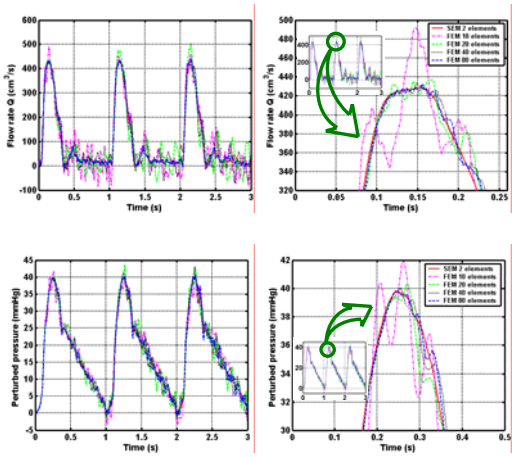

Fig. 5. Comparison of the blood flow rate and pressure obtained by using the present SEM and the conventional FEM for the uniform flow.

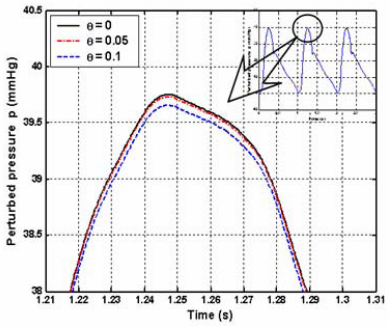

Fig. 6. The perturbed blood pressure vs. the taper of the cross-sectional area of blood vessel for the uniform flow.

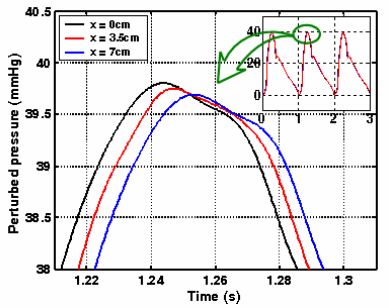

Fig. 7. The perturbed blood pressures at different locations (x = 0, 3.5, 7 cm) for the uniform flow.

Fig. 7 that the magnitude of blood pressure decreases as the blood flows downwards due to the effects of blood viscosity.

As the cardiovascular system is a huge network of blood vessels, the length of a blood vessel originating from the heart can be considered semi-infinite. In the element methods such as the conventional FEM and the present SEM, it is not always easy to deal with such semi-infinite length of blood vessel. So it may be important to investigate the effects of the finite length of blood vessel on the predicted characteristics of blood flow. To this end, Fig. 8 shows the blood flow rates and blood pressures (at x = 3.5 cm) for different total lengths of blood vessel. As expected, the shortest blood vessel shows the strongest effects of the wave reflection at the far down end of blood vessel. As the total length of a blood vessel is increased, the effects of wave reflection are getting smaller to smooth the curves of the blood flow rate and blood pressure. This implies that it is important to accurately take into account the effects of wave reflection at the far down end of a blood vessel to get more accurate blood flow characteristics within the blood vessel.

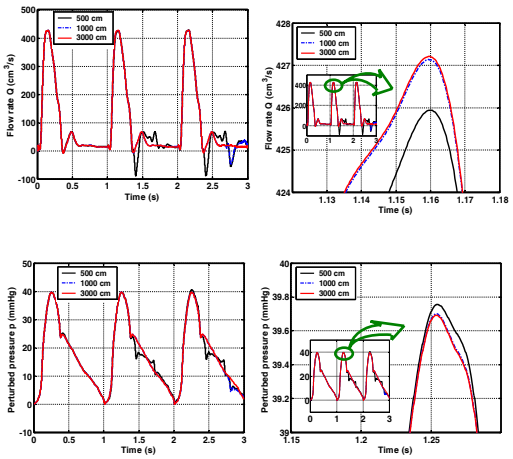

Fig. 8. The blood flow rates and perturbed blood pressures at x = 3.5 cm for different lengths of blood vessel for the uniform flow.

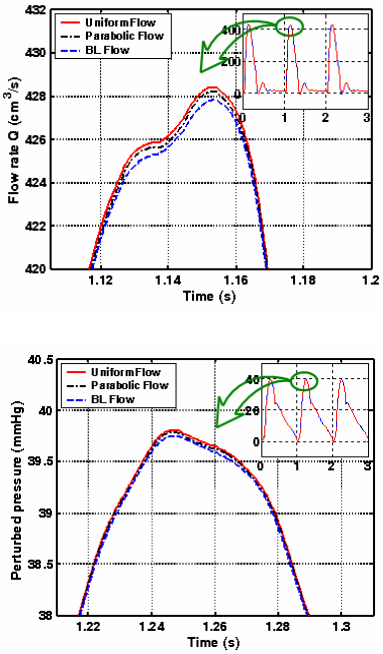

Fig. 9. The blood flow rates and perturbed blood pressures at x = 3.5 cm for different blood flow velocity profiles: uniform flow, parabolic flow and boundary layer (BL) flow.

The blood flow velocity profile may depend on the fluid properties of blood (i.e., viscosity, density, etc.) as well as on the geometry of blood vessel. Thus, we considered three types of blood flow velocity profiles as shown in Fig. 3. The blood flow rate and blood pressure at x = 3.5 cm for each blood flow velocity profile are compared in Fig. 9. For the case of bound-

ary layered flow, the boundary layer thickness δ = 0.125 cm is used. Though there is no significant difference between blood flow velocity files, the uniform flow profile seems to provide the largest blood flow rate and blood pressure, while the boundary layered flow profile provides the smallest values.

5. Conclusion

In this paper, a one-dimensional spectral element model is developed for human blood vessels with slowly varying cross-sections. The spectral element is formulated by using the wave solutions satisfying governing equations in frequency-domain as the frequency-dependent interpolation functions. The spectral element model is then applied to a blood vessel to investigate the blood flow rate and pressure for various flow velocity profiles. It is numerically shown that the present spectral element model provides realistic blood flow through the example blood vessel considered in this study. It is also investigated that the length of blood vessel is somewhat important to successfully take into account the effects of the blood waves reflected from the downstream end of blood vessels.

Acknowledgement

This work was supoorted by the Korea Research Foundation Grant funded by the Korean Government (MOEHRD) (KRF-2005-041-D00042).

References

[1] J. R. Wormersly, Oscillatory flow in arteries: the constrained elastic tube as a model of arterial flow and pulse transmission, *Physics in Medicine and Biology* 7 (1957) 178-187.

[2] T. J. R. Hughes and J. Lubliner, On the one-dimensional theory of blood flow in the larger vessels, *Mathematical Biosciences* 18 (1973) 161-170.

[3] M. S. Olufsen, Structured tree outflow condition for blood flow in larger systemic arteries, *American Journal of Physiology* 276 (1999) H257-H268.

[4] L. Formaggia, J. F. Gerbeau, F. Nobile and A. Quarteroni, On the coupling of 3D and 1D Navier-Stokes equations for flow problems in compliant vessels, *Computer Methods in Applied Mechanics and Engineering* 191 (2001) 561-582.

[5] K. Laganà, G. Dubini, F. Migliavacca, R. Pietrabissa G. Pennati, A. Veneziani and A. Quarteroni, Multiscale modeling as a tool to prescribe realistic boundary conditions for the study of surgical procedures, *Biorheology* 39 (2002) 359-364.

[6] J. Wan, B. Steele, S. A. Spicer, S. Strohband, G. R. Feijoo, T. J. R. Hughes and C. A. Taylor, A one-dimensional finite element method for simulation-based medical planning for cardiocascular disease, *Computer Methods in Biomechanics and Biomedical Engineering* 5(3) (2002) 195-206.

[7] B. N. Steele, J. Wan, J. P. Ku, T. J. R. Hughes and C. A. Taylor, In vivo validation of a one-dimensional finite-element method of predicting blood flow in cardiovascular bypass grafts, *IEEE Transactions on Biomedical Engineering* 50(6) (2003) 649-656.

[8] I. E. Vignon and C. A. Taylor, Outflow boundary conditions for one-dimensional finite element modeling of blood flow and pressure waves in arteries, *Wave Motion* 39 (2004) 361-374.

[9] S. J. Sherwin, V. Franke and J. Peiro, One-dimensional modelling of a vascular network in space-time variables, *Journal of Engineering Mathematics* 47 (2003) 217-250.

[10] J. F. Doyle, Wave Propagation in Structures: Spectral Analysis Using Fast Discrete Fourier Transforms, Springer, New York, USA, (1997).

[11] U. Lee, Spectral Element Method in Structural Dynamics, Inha University Press, Inha University, Incheon, Korea, (2004).

[12] U. Lee, B. Seo and I. Jang, Blood flow analysis by using spectral element method, *Dynamics of Continuous, Discrete & Impulse Systems, Series B: Applications & Algoritms* 14(S4) (2007) 180-184.

[13] D. E. Newland, Random Vibrations, Spectral and Wavelet Analysis, Longman, New York, USA, (1993).

Appendix

A: Finite element model

The finite element model used in this study is formulated by using the flow fields assumed as

$$\begin{aligned} Q(x,t) &= \left[\boldsymbol{N}(x)\right]\left\{\boldsymbol{Q}(t)\right\} \\ p(x,t) &= \left[\boldsymbol{N}(x)\right]\left\{\boldsymbol{p}(t)\right\} \end{aligned} \tag{A1}$$

where

$$\left[\boldsymbol{N}(x)\right]=\left[1-x/l \quad x/l\right] \tag{A2}$$

By substituting Eq. (A1) into the weak forms of Eqs. (5) and (6), we get the finite element equations as follows:

$$\begin{aligned}&[\boldsymbol{M}]\{\ddot{\boldsymbol{Q}}(t)\}+[\boldsymbol{C}]\{\dot{\boldsymbol{Q}}(t)\}+[\boldsymbol{K}]\{\boldsymbol{Q}(t)\}=\{\boldsymbol{f}_Q(p,Q;t)\}\\&[\boldsymbol{M}]\{\ddot{\boldsymbol{p}}(t)\}+[\boldsymbol{C}]\{\dot{\boldsymbol{p}}(t)\}+[\boldsymbol{K}]\{\boldsymbol{p}(t)\}=\{\boldsymbol{f}_p(p,Q;t)\}\end{aligned} \tag{A3}$$

where

$$\begin{aligned}&\{\boldsymbol{f}_Q(p,Q;t)\}=[\boldsymbol{C}_{NLQ}(\boldsymbol{p})]\{\dot{\boldsymbol{Q}}(t)\}-[\boldsymbol{K}_{NLQ}(\boldsymbol{p},\dot{\boldsymbol{Q}})]\{\boldsymbol{Q}(t)\}+\{f_{Q1}\quad f_{Q2}\}^{\mathrm{T}}\\&\{\boldsymbol{f}_p(p,Q;t)\}=[\boldsymbol{C}_{NLp}(\boldsymbol{Q})]\{\dot{\boldsymbol{p}}(t)\}-[\boldsymbol{K}_{NLp}(\boldsymbol{p},\dot{\boldsymbol{p}},\dot{\boldsymbol{Q}})]\{\boldsymbol{p}(t)\}+\{f_{p1}\quad f_{p2}\}^{\mathrm{T}}\end{aligned} \tag{A4}$$

with the use of definitions as

$$[\boldsymbol{M}]=\int_0^l\left[\boldsymbol{N}(x)\right]^T\left[\boldsymbol{N}(x)\right]dx$$

$$[\boldsymbol{K}]=a_1\int_0^l\left[\boldsymbol{N}'(x)\right]^T\left[\boldsymbol{N}'(x)\right]dx$$

$$[\boldsymbol{C}]=a_2\int_0^l\left[\boldsymbol{N}(x)\right]^T\left[\boldsymbol{N}(x)\right]dx+a_3\int_0^l\left[\boldsymbol{N}'(x)\right]^T\left[\boldsymbol{N}'(x)\right]dx$$

$$\left[\boldsymbol{C}_{NLQ}\right]=a_6\int_0^l\left[\boldsymbol{N}(x)\right]^T\left\{p(t)\right\}^T\left[\boldsymbol{N}(x)\right]^T\left[\boldsymbol{N}(x)\right]dx$$

$$\begin{aligned}\left[\boldsymbol{C}_{NLp}\right]=&-2a_4\int_0^l\left[\boldsymbol{N}(x)\right]^T\left\{\boldsymbol{Q}(t)\right\}^T\left[\boldsymbol{N}(x)\right]^T\left[\boldsymbol{N}(x)\right]dx\\&+a_5\int_0^l\left[\boldsymbol{N}'(x)\right]^T\left\{Q(t)\right\}^T\left[\boldsymbol{N}(x)\right]^T\left[\boldsymbol{N}(x)\right]dx\end{aligned}$$

$$\begin{aligned}\left[\boldsymbol{K}_{NLQ}\right]=&\,2a_4\int_0^l\left[\boldsymbol{N}(x)\right]^T\left\{\dot{\boldsymbol{Q}}(t)\right\}^T\left[\boldsymbol{N}(x)\right]^T\left[\boldsymbol{N}(x)\right]dx\\&+a_5\int_0^l\left[\boldsymbol{N}(x)\right]^T\left\{\dot{\boldsymbol{Q}}(t)\right\}^T\left[\boldsymbol{N}(x)\right]^T\left[\boldsymbol{N}'(x)\right]dx\\&+a_5\int_0^l\left[\boldsymbol{N}(x)\right]^T\left\{\dot{\boldsymbol{Q}}(t)\right\}^T\left[\boldsymbol{N}'(x)\right]^T\left[\boldsymbol{N}(x)\right]dx\\&+a_1a_6a_0^{-1}\int_0^l\left[\boldsymbol{N}(x)\right]^T\left\{\boldsymbol{Q}(t)\right\}^T\left[\boldsymbol{N}'(x)\right]^T\left[\boldsymbol{N}(x)\right]dx\\&+a_1a_7a_0^{-1}\int_0^l\left[\boldsymbol{N}'(x)\right]^T\left\{\boldsymbol{p}(t)\right\}^T\left[\boldsymbol{N}(x)\right]^T\left[\boldsymbol{N}'(x)\right]dx\\&+(a_1a_8-2a_1a_{10})a_0^{-1}\int_0^l\left[\boldsymbol{N}(x)\right]^T\left\{\boldsymbol{Q}(t)\right\}^T\left[\boldsymbol{N}'(x)\right]^T\left\{\boldsymbol{Q}(t)\right\}^T\left[\boldsymbol{N}'(x)\right]^T\left[\boldsymbol{N}(x)\right]dx\\&-a_8\int_0^l\left[\boldsymbol{N}(x)\right]^T\left\{\boldsymbol{p}(t)\right\}^T\left[\boldsymbol{N}(x)\right]^T\left\{\dot{\boldsymbol{Q}}(t)\right\}^T\left[\boldsymbol{N}(x)\right]^T\left[\boldsymbol{N}'(x)\right]dx\\&-a_8\int_0^l\left[\boldsymbol{N}(x)\right]^T\left\{\boldsymbol{p}(t)\right\}^T\left[\boldsymbol{N}(x)\right]^T\left\{\dot{\boldsymbol{Q}}(t)\right\}^T\left[\boldsymbol{N}'(x)\right]^T\left[\boldsymbol{N}(x)\right]dx\\&+a_1a_9a_0^{-1}\int_0^l\left[\boldsymbol{N}(x)\right]^T\left\{\boldsymbol{Q}(t)\right\}^T\left[\boldsymbol{N}'(x)\right]^T\left\{Q(t)\right\}^T\left[\boldsymbol{N}(x)\right]^T\left[\boldsymbol{N}(x)\right]dx\\&-2a_9\int_0^l\left[\boldsymbol{N}(x)\right]^T\left\{\boldsymbol{p}(t)\right\}^T\left[\boldsymbol{N}(x)\right]^T\left\{\dot{Q}(t)\right\}^T\left[\boldsymbol{N}(x)\right]^T\left[\boldsymbol{N}(x)\right]dx\\&-a_1a_{10}a_0^{-1}\int_0^l\left[\boldsymbol{N}'(x)\right]^T\left\{\boldsymbol{Q}(t)\right\}^T\left[\boldsymbol{N}'(x)\right]^T\left\{\boldsymbol{Q}(t)\right\}^T\left[\boldsymbol{N}(x)\right]^T\left[\boldsymbol{N}(x)\right]dx\\&-2a_{10}\int_0^l\left[\boldsymbol{N}(x)\right]^T\left\{\boldsymbol{p}(t)\right\}^T\left[\boldsymbol{N}'(x)\right]^T\left\{\dot{\boldsymbol{Q}}(t)\right\}^T\left[\boldsymbol{N}(x)\right]^T\left[\boldsymbol{N}(x)\right]dx\end{aligned}$$

$$\begin{aligned}\left[\boldsymbol{K}_{NLp}\right]=&\,a_1a_6a_0^{-1}\int_0^l\left[\boldsymbol{N}(x)\right]^T\left\{\boldsymbol{Q}(t)\right\}^T\left[\boldsymbol{N}(x)\right]^T\left[\boldsymbol{N}'(x)\right]dx\\&-a_6\int_0^l\left[\boldsymbol{N}(x)\right]^T\left\{\dot{\boldsymbol{p}}(t)\right\}^T\left[\boldsymbol{N}(x)\right]^T\left[\boldsymbol{N}(x)\right]dx\\&+a_1a_7a_0^{-1}\int_0^l\left[\boldsymbol{N}'(x)\right]^T\left\{\boldsymbol{p}(t)\right\}^T\left[\boldsymbol{N}(x)\right]^T\left[\boldsymbol{N}'(x)\right]dx\\&+(a_{10}-a_8)\int_0^l\left[\boldsymbol{N}(x)\right]^T\left\{\boldsymbol{Q}(t)\right\}^T\left[\boldsymbol{N}(x)\right]^T\left\{\dot{\boldsymbol{p}}(t)\right\}^T\left[\boldsymbol{N}(x)\right]^T\left[\boldsymbol{N}'(x)\right]dx\\&+a_0a_8a_1^{-1}\int_0^l\left[\boldsymbol{N}(x)\right]^T\left\{\dot{\boldsymbol{p}}(t)\right\}^T\left[\boldsymbol{N}(x)\right]^T\left\{\dot{\boldsymbol{p}}(t)\right\}^T\left[\boldsymbol{N}(x)\right]^T\left[\boldsymbol{N}(x)\right]dx\\&-a_0a_{10}a_1^{-1}\int_0^l\left[\boldsymbol{N}(x)\right]^T\left\{\dot{\boldsymbol{p}}(t)\right\}^T\left[\boldsymbol{N}(x)\right]^T\left\{\dot{\boldsymbol{p}}(t)\right\}^T\left[\boldsymbol{N}(x)\right]^T\left[\boldsymbol{N}'(x)\right]dx\\&+a_{10}\int_0^l\left[\boldsymbol{N}'(x)\right]^T\left\{\boldsymbol{Q}(t)\right\}^T\left[\boldsymbol{N}(x)\right]^T\left\{\dot{\boldsymbol{p}}(t)\right\}^T\left[\boldsymbol{N}(x)\right]^T\left[\boldsymbol{N}(x)\right]dx\\&+a_1a_9a_0^{-1}\int_0^l\left[\boldsymbol{N}(x)\right]^T\left\{\boldsymbol{Q}(t)\right\}^T\left[\boldsymbol{N}(x)\right]^T\left\{\boldsymbol{Q}(t)\right\}^T\left[\boldsymbol{N}(x)\right]^T\left[\boldsymbol{N}'(x)\right]dx\\&-2a_9\int_0^l\left[\boldsymbol{N}(x)\right]^T\left\{\dot{\boldsymbol{p}}(t)\right\}^T\left[\boldsymbol{N}(x)\right]^T\left\{\boldsymbol{Q}(t)\right\}^T\left[\boldsymbol{N}(x)\right]^T\left[\boldsymbol{N}(x)\right]dx\\&-a_1a_{10}a_0^{-1}\int_0^l\left[\boldsymbol{N}'(x)\right]^T\left\{\boldsymbol{Q}(t)\right\}^T\left[\boldsymbol{N}(x)\right]^T\left\{\boldsymbol{Q}(t)\right\}^T\left[\boldsymbol{N}(x)\right]^T\left[\boldsymbol{N}'(x)\right]dx\end{aligned}$$

$$\begin{aligned}f_{Q1}&=\left(a_1Q'+a_3\dot{Q}'+a_1a_7a_0^{-1}pQ'-a_1a_{10}a_0^{-1}Q'Q^2\right)\Big|_{x=0}\\f_{Q2}&=\left(a_1Q'+a_3\dot{Q}'+a_1a_7a_0^{-1}pQ'-a_1a_{10}a_0^{-1}Q'Q^2\right)\Big|_{x=l}\\f_{p1}&=\left(a_1p'+a_3\dot{p}'+a_1a_7a_0^{-1}pp'-a_1a_{10}a_0^{-1}p'Q^2-2a_5\dot{p}Q+a_{10}p\dot{p}Q\right)\Big|_{x=0}\\f_{p2}&=\left(a_1p'+a_3\dot{p}'+a_1a_7a_0^{-1}pp'-a_1a_{10}a_0^{-1}p'Q^2-2a_5\dot{p}Q+a_{10}p\dot{p}Q\right)\Big|_{x=l}\end{aligned} \tag{A5}$$